

# LOSTU: Fast, Scalable, and Uncertainty-Aware Triangulation

Sébastien Henry and John A. Christian

Daniel Guggenheim School of Aerospace Engineering  
Georgia Institute of Technology, Atlanta, GA 30332, USA

seb.henry@gatech.edu, john.a.christian@gatech.edu

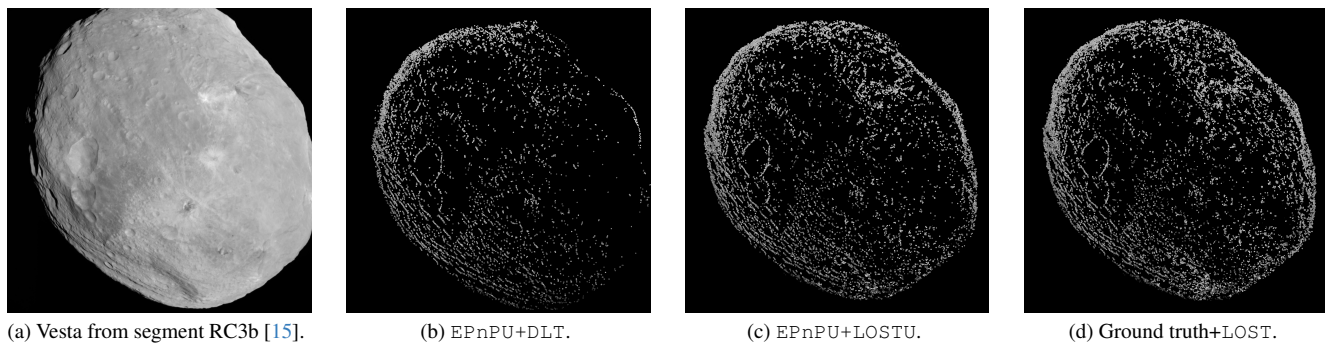


Figure 1. Reconstruction of the asteroid Vesta from images of the RC3b phase of the Dawn mission. For the same constraint on the maximum covariance of a reconstructed point, the maximum likelihood triangulation method is able to reconstruct more points.

## Abstract

Triangulation algorithms often aim to minimize the reprojection ( $L_2$ ) error, but this only provides the maximum likelihood estimate when there are no errors in the camera parameters or camera poses. Although recent advances have yielded techniques to estimate camera parameters accounting for 3D point uncertainties, most structure from motion (SfM) pipelines still use older triangulation algorithms. This work leverages recent discoveries to provide a fast, scalable, and statistically optimal way to triangulate called *LOSTU*. Results show that *LOSTU* consistently produces lower 3D reconstruction errors than conventional  $L_2$  triangulation methods—often allowing *LOSTU* to successfully triangulate more points. Moreover, in addition to providing a better 3D reconstruction, *LOSTU* can be substantially faster than Levenberg-Marquardt (or similar) optimization schemes.

## 1. Introduction

Triangulation describes the task of localizing a point by the intersection of two—or more—lines-of-position (LOPs). In computer vision applications, these LOPs usually originate from line-of-sight (LOS) directions that are transformed

from a camera frame into the world frame. Such situations arise naturally in image-based 3D reconstruction and navigation problems. Although practical triangulation algorithms have been around for hundreds of years [26], it remains a problem of contemporary study.

Several important points are to be considered when choosing a triangulation method: its optimality, its scalability to multiple views, and its projective invariance property. It can be shown that under the assumption of Gaussian 2D noise, the solution minimizing the reprojection error provides the maximum likelihood estimate and is projective invariant [23]. This type of approach is often named  $L_2$  or *optimal* triangulation, but this cost function is difficult to work with because it has multiple local minima [25]—unlike  $L_\infty$  triangulation [22, 30] that has a single local (and thus global) minimum.

In 2-view triangulation, the optimal solution can be found by solving for the root of a sixth-order polynomial [25], and faster alternative methods exist [31, 38]. Yet, the problem quickly becomes intractable as more views are added. It is, for example, necessary to find the roots of a 47th degree polynomial for 3 views [53]. Some notable work has also been done to speed up 3-view triangulation [4, 34] but is not scalable to more points. Triangulation algorithms like the direct linear transform (DLT) [23] and the

midpoint method [25] are popular due to their scalability to multiple views. These, or  $L_\infty$  triangulation [42], are often used to obtain an initial estimate that is then iteratively refined to minimize the reprojection error. However, the refinement can be slow and may not converge to the global optimum. Subsequent methods—like the linear optimal sine triangulation (LOST)—yield a closed-form, fast, and scalable solution to  $L_2$  triangulation by weighting the DLT [26]. This framework has been shown to give statistically similar results to the common iterative optimal approach [33].

Understanding the limitations of  $L_2$  triangulation is essential. First, there are certain geometries (typically symmetric geometries) under which all triangulation methods perform similarly [25, 26] and hence where optimal triangulation does not offer substantial performance gains. Furthermore, geometries involving low-parallax are a typical example where  $L_2$  triangulation performs poorly [25, 35]. Regardless,  $L_2$  triangulation can provide substantial improvements over sub-optimal methods in general scenarios that are not symmetric and don't have low parallax [25, 26].

Second, minimizing the reprojection error is only optimal under the assumptions of Gaussian 2D noise on the image measurements and perfect knowledge of the camera parameters. Reference [45] argues that the midpoint method should be used over  $L_2$  optimal triangulation in the SfM process because of uncertainties in the extrinsic camera parameters. However, the midpoint remains a method that inherently minimizes the wrong cost function. A more appropriate approach under camera parameter uncertainties is to modify the  $L_2$  cost function in the iterative refinement process, as it is done in Ref. [3, 20, 36]. Spurred by the challenges in spacecraft localization, the authors of the LOST algorithm developed a method to account for the effects of planetary uncertainty and spacecraft camera attitude uncertainties, and how to treat them optimally in the LOST triangulation solution [27]. The algorithm once again features a linear system, but no numerical simulation to validate that method has been done in Ref. [27] since it was concluded that these effects were mostly negligible in spaceflight.

This paper aims to carefully study triangulation under camera pose uncertainty and address performance effects with traditional triangulation methods. It does so by continuing the work of Refs. [26, 27] while simultaneously presenting it to the computer vision community. We show that LOST can be used in an intersection problem where the “planetary position uncertainties” become the “camera center uncertainties”. Because Ref. [45] did not consider any uncertain optimal triangulation methods in their work and Ref. [20] only used a refinement step as a part of a broader SfM pipeline, few studies have isolated the effect of taking camera parameter uncertainties into account in triangulation. We thus perform numerical simulations to experimentally validate LOST and assess the benefits of con-

sidering camera parameters uncertainties. It will be shown that LOST can be used as by itself or as a non-iterative alternative to Levenberg-Marquardt refinement. The benefits of taking camera parameter uncertainties into account are demonstrated in a maximum likelihood SfM pipeline.

## 2. Linear optimal sine framework

This work utilizes the pinhole camera model. For simplicity of notation, we denote the vector  $\mathbf{k} = [0, 0, 1]^T$ . Then, the homogeneous pixel coordinate measurement of point  $i$  in view  $j$  is often represented as

$$\mathbf{x}_{ij} = \frac{\mathbf{K}_j \mathbf{R}_{C_j}^W (\mathbf{X}_i - \mathbf{c}_j)}{\mathbf{k}^T \mathbf{K}_j \mathbf{R}_{C_j}^W (\mathbf{X}_i - \mathbf{c}_j)}, \quad (1)$$

where  $\mathbf{K}_j$  is the camera calibration matrix,  $\mathbf{x}_{ij}$  is the 2D measurement of the object in homogeneous coordinates,  $\mathbf{R}_{C_j}^W$  is the rotation matrix from world frame to camera frame,  $\mathbf{X}_i$  is the 3D world position of the measured object, and  $\mathbf{c}_j$  is the 3D world position of the camera. The reader will recognize that, under perfect measurement, the measurement vector should be colinear to the line-of-sight

$$\mathbf{K}_j^{-1} \mathbf{x}_{ij} \propto \rho_{ij} \frac{\mathbf{K}_j^{-1} \mathbf{x}_{ij}}{\|\mathbf{K}_j^{-1} \mathbf{x}_{ij}\|} = \rho_{ij} \mathbf{a}_{ij} = \mathbf{R}_{C_j}^W (\mathbf{X}_i - \mathbf{c}_j), \quad (2)$$

where  $\rho_{ij} = \|\mathbf{X}_i - \mathbf{c}_j\|$  is the range and  $\mathbf{a}_{ij}$  is the unit vector in the direction of the measurement in the camera frame. Thus, the cross product between those two vectors results in the zero vector (a vector writing of the law of sines). In practice, the 2D measurements are perturbed by noise, often assumed Gaussian, and this leads to the equation for the law of sines residual

$$\boldsymbol{\epsilon}_{ij} = [\mathbf{K}_j^{-1} \mathbf{x}_{ij} \times] \mathbf{R}_{C_j}^W (\mathbf{X}_i - \mathbf{c}_j). \quad (3)$$

where  $[\cdot \times]$  is the skew symmetric cross product matrix  $\mathbf{a} \times \mathbf{b} = [\mathbf{a} \times] \mathbf{b}$ . The partials of  $\boldsymbol{\epsilon}_{ij}$  with respect to the 2D measurement are

$$\mathbf{J}_{\mathbf{x}_{ij}} = \partial \boldsymbol{\epsilon}_{ij} / \partial \mathbf{x}_{ij} = -[\mathbf{R}_{C_j}^W (\mathbf{X}_i - \mathbf{c}_j) \times] \mathbf{K}_j^{-1}. \quad (4)$$

Similarly, the partials with respect to the extrinsic camera parameters can be obtained as Ref. [27]:

$$\mathbf{J}_{\mathbf{c}_j} = \partial \boldsymbol{\epsilon}_{ij} / \partial \mathbf{c}_j = -[\mathbf{K}_j^{-1} \mathbf{x}_{ij} \times] \mathbf{R}_{C_j}^W, \quad (5a)$$

$$\mathbf{J}_{\phi_j} = \partial \boldsymbol{\epsilon}_{ij} / \partial \phi_j = [\mathbf{K}_j^{-1} \mathbf{x}_{ij} \times] [\mathbf{R}_{C_j}^W (\mathbf{X}_i - \mathbf{c}_j) \times], \quad (5b)$$

where  $\phi_j$  is the angle-vector description of a rotation perturbation in  $\mathbf{R}_{C_j}^W$ . The partials with respect to the 3D world positions are

$$\mathbf{J}_{\mathbf{X}_i} = \partial \boldsymbol{\epsilon}_{ij} / \partial \mathbf{X}_i = [\mathbf{K}_j^{-1} \mathbf{x}_{ij} \times] \mathbf{R}_{C_j}^W. \quad (6)$$

Because the inverse of the calibration matrix has a simple closed-form [8], we can take the partials with respect to the desired intrinsic parameters as

$$\mathbf{J}_{K_j[l,m]} = \frac{\partial \epsilon_{ij}}{\partial K_j^{-1}} = -[\mathbf{R}_{C_i}^W(\mathbf{X}_i - \mathbf{c}_j) \times] \frac{\partial K_j^{-1}}{\partial K_j[l,m]} \mathbf{x}_{ij}, \quad (7)$$

where  $K_j[l,m]$  is the  $l, m$ -th entry of the calibration matrix. The partials to other calibration parameters such as the radial distortion could also be taken into account by taking the appropriate Jacobians.

Assuming uncorrelated Gaussian noise models where  $\Sigma_{(\cdot)}$  represent the covariance matrix of  $(\cdot)$ , Eqs. (4), (5a), (5b), (6) and (7) make it possible to project the individual parameter uncertainties onto the residual uncertainties as

$$\Sigma_{\epsilon_{ij}} = \mathbf{J}_{\phi_j} \Sigma_{\phi_j} \mathbf{J}_{\phi_j}^T + \mathbf{J}_{\mathbf{x}_{ij}} \Sigma_{\mathbf{x}_{ij}} \mathbf{J}_{\mathbf{x}_{ij}}^T + \dots \quad (8)$$

Denote the set of points visible in view  $j$  as  $\mathcal{V}_j$ . The MLE is the solution that minimizes the cost function

$$J(\mathbf{K}, \mathbf{R}, \mathbf{c}, \mathbf{x}, \mathbf{X}) = \sum_j \sum_{i \in \mathcal{V}_j} \epsilon_{ij}^T \Sigma_{\epsilon_{ij}}^{-1} \epsilon_{ij}. \quad (9)$$

Due to the fact that the first cross product in Eq. (4) to Eq. (7) have the same null space, the matrix  $\Sigma_{\epsilon_{ij}}$  is not full rank and thus not invertible. The trick resides in observing that the null space of  $\Sigma_{\epsilon_{ij}}$  naturally aligns with the residual of Eq. (3), and one can thus use the pseudo-inverse  $\Sigma_{\epsilon_{ij}}^\dagger$  instead of the matrix inversion to rewrite Eq. (9) as

$$J(\mathbf{K}, \mathbf{R}, \mathbf{c}, \mathbf{x}, \mathbf{X}) = \sum_j \sum_{i \in \mathcal{V}_j} \epsilon_{ij}^T \Sigma_{\epsilon_{ij}}^\dagger \epsilon_{ij}. \quad (10)$$

## 2.1. Linear optimal sine triangulation (LOST)

Denote the track as the set  $\mathcal{T}_i$  that consists of all the views that see the  $i$ th point,  $\mathcal{T}_i = \{j : i \in \mathcal{V}_j\}$ . In the case of intersection, we seek to estimate the point  $\mathbf{X}_i$ , and the cost function in Eq. (10) becomes

$$J(\mathbf{X}_i) = \sum_{j \in \mathcal{T}_i} \epsilon_{ij}^T \Sigma_{\epsilon_{ij}}^\dagger \epsilon_{ij} \quad (11)$$

where  $\Sigma_{\epsilon_{ij}}$  is computed using Eq. (8), but does not take the partial derivative at Eq. (6) into consideration. If an initial estimate for the 3D point exists, then it is straightforward to compute the Jacobians. When no *a-priori* information is available, the covariance of the residual can still be computed. We can start by the acknowledging that

$$[\mathbf{R}_{C_i}^W(\mathbf{X}_i - \mathbf{c}_j) \times] = \rho_{ij} [\mathbf{a}_{ij} \times]. \quad (12)$$

Given that the camera centers are known (in intersection), the range  $\rho_{ij} = \|\mathbf{X}_i - \mathbf{c}_j\|$  can be computed with the help

of another measurement  $\mathbf{x}_{ij'}$  using the law of sines [26]

$$\rho_{ij} = \frac{\|\mathbf{R}_{C_i}^W(\mathbf{c}_j - \mathbf{c}_{j'}) \times \mathbf{a}_{ij}\|}{\|\mathbf{a}_{ij} \times \mathbf{a}_{ij'}\|}. \quad (13)$$

The optimal point is the point satisfying  $\partial J(\mathbf{X}_i)/\partial \mathbf{X}_i = \mathbf{0}$ , which yields the final system to triangulate the position of the  $i$ th 3D point [26]

$$\begin{aligned} & \left( \sum_{j \in \mathcal{T}_i} \mathbf{R}_W^{C_j} [\mathbf{K}_j^{-1} \mathbf{x}_{ij} \times] \Sigma_{\epsilon_{ij}}^\dagger [\mathbf{K}_j^{-1} \mathbf{x}_{ij} \times] \mathbf{R}_{C_j}^W \right) \mathbf{X}_i \\ &= \sum_{j \in \mathcal{T}_i} \mathbf{R}_W^{C_j} [\mathbf{K}_j^{-1} \mathbf{x}_{ij} \times] \Sigma_{\epsilon_{ij}}^\dagger [\mathbf{K}_j^{-1} \mathbf{x}_{ij} \times] \mathbf{R}_{C_j}^W \mathbf{c}_j. \end{aligned} \quad (14)$$

Assuming isotropic 2D noise only ( $\Sigma_{\mathbf{x}_{ij}} = \sigma_{\mathbf{x}_{ij}}^2 \mathbf{I}_{2 \times 2}$ ), the system can be further simplified by the QR factorization of the  $\Sigma_{\epsilon_{ij}}^\dagger$ . Denote the weights [26]

$$q_j = \frac{\|\mathbf{K}_j^{-1} \mathbf{x}_{ij}\|}{\mathbf{K}^{-1}[0,0] \sigma_{\mathbf{x}_{ij}} \rho_{ij}}, \quad (15)$$

where  $\rho_{ij}$  can be computed with Eq. (13). The system to solve can be rewritten as [26]

$$\begin{bmatrix} q_1 S [\mathbf{K}_{j_1}^{-1} \mathbf{x}_{ij_1} \times] \mathbf{R}_{C_{j_1}}^W \\ q_2 S [\mathbf{K}_{j_2}^{-1} \mathbf{x}_{ij_2} \times] \mathbf{R}_{C_{j_2}}^W \\ \vdots \\ q_n S [\mathbf{K}_{j_n}^{-1} \mathbf{x}_{ij_n} \times] \mathbf{R}_{C_{j_n}}^W \end{bmatrix} \mathbf{X}_i = \begin{bmatrix} q_1 S [\mathbf{K}_{j_1}^{-1} \mathbf{x}_{ij_1} \times] \mathbf{R}_{C_{j_1}}^W \mathbf{c}_{j_1} \\ q_2 S [\mathbf{K}_{j_2}^{-1} \mathbf{x}_{ij_2} \times] \mathbf{R}_{C_{j_2}}^W \mathbf{c}_{j_2} \\ \vdots \\ q_n S [\mathbf{K}_{j_n}^{-1} \mathbf{x}_{ij_n} \times] \mathbf{R}_{C_{j_n}}^W \mathbf{c}_{j_n} \end{bmatrix} \quad (16)$$

,  $\{j_1, \dots, j_n\} \in \mathcal{T}_i$ . Eq. (15) is an important function that can help us understand when optimal triangulation matters most over the DLT. The DLT solution is obtained by solving the system Eq. (14) replacing all  $\Sigma_{\epsilon_{ij}}$  by  $\mathbf{I}_{3 \times 3}$ , or Eq. (14) replacing all  $q_j$  by a constant. Therefore, we observe that the optimal solution will differ from that of the DLT when the measurement range to the 3D point, or the 2D noise, varies between different views.

In the rest of the paper, we refer to LOST as the algorithm that solves Eq. (16), *i.e.* that only accounts for 2D uncertainties. We refer to LOSTU as the algorithm that solves Eq. (14), *i.e.* accounting for uncertainties of camera parameters and 2D noise. Neither LOST or LOSTU use an *a-priori* estimate of  $\mathbf{X}_i$ , as they find the range with Eq. (13). The algorithm DLT refers to Eq. (16) where all  $q_j = 1$ . The covariance of a point — accounting for both 2D and camera uncertainties — triangulated with linear triangulation methods like DLT, LOST, and LOSTU can be found at negligible computational expense, and expressions are in Ref. [26].

## 2.2. Optimal camera center estimation

The underlying analysis for resection (*e.g.* in navigation) is identical to the one in Sec. 2.1. Consider the cost function

$$J(\mathbf{c}_j) = \sum_{i \in \mathcal{V}_j} \epsilon_{ij}^T \Sigma_{\epsilon_{ij}}^\dagger \epsilon_{ij}, \quad (17)$$

Then the optimal camera center  $\mathbf{c}_j$  is found with

$$\begin{aligned} & \left( \sum_{i \in \mathcal{V}_j} \mathbf{R}_W^{C_j} [\mathbf{K}_j^{-1} \mathbf{x}_{ij} \times] \Sigma_{\epsilon_{ij}}^\dagger [\mathbf{K}_j^{-1} \mathbf{x}_{ij} \times] \mathbf{R}_{C_j}^W \right) \mathbf{c}_j \\ &= \sum_{i \in \mathcal{V}_j} \mathbf{R}_W^{C_j} [\mathbf{K}_j^{-1} \mathbf{x}_{ij} \times] \Sigma_{\epsilon_{ij}}^\dagger [\mathbf{K}_j^{-1} \mathbf{x}_{ij} \times] \mathbf{R}_{C_j}^W \mathbf{X}_i. \end{aligned} \quad (18)$$

### 2.3. Optimality of midpoint

Some experiments have found that midpoint performs well when triangulating with camera pose noise [45], but little explanation is provided to rationalize those results. Starting from Eq. (14), we show that the midpoint is the optimal method when, 1) all cameras have the same position covariance, and 2) this camera position uncertainty dominates all other error sources. In this case, using Eq. (5a) and Eq. (8), the covariance of  $\epsilon_{ij}$  is

$$\Sigma_{\epsilon_{ij}} = -[\mathbf{K}_j^{-1} \mathbf{x}_{ij} \times] \mathbf{R}_{C_j}^W \Sigma_{\mathbf{c}_j} \mathbf{R}_W^{C_j} [\mathbf{K}_j^{-1} \mathbf{x}_{ij} \times], \quad (19)$$

where we considered the fact that  $[\cdot \times]^T = -[\cdot \times]$ . Assuming an isotropic camera center noise under the form  $\Sigma_{\mathbf{c}_j} = \mathbf{I}$ , and noting  $\mathbf{R}_{C_j}^W \mathbf{R}_W^{C_j} = \mathbf{I}$ , we compute its pseudo-inverse as

$$\Sigma_{\epsilon_{ij}}^\dagger = -\frac{1}{\|\mathbf{K}_j^{-1} \mathbf{x}_{ij} \times\|^4} [\mathbf{K}_j^{-1} \mathbf{x}_{ij} \times]^2. \quad (20)$$

It follows that

$$\mathbf{R}_W^{C_j} [\mathbf{K}_j^{-1} \mathbf{x}_{ij} \times] \Sigma_{\epsilon_{ij}}^\dagger [\mathbf{K}_j^{-1} \mathbf{x}_{ij} \times] \mathbf{R}_{C_j}^W = \mathbf{R}_W^{C_j} [\mathbf{a}_{ij} \times]^4 \mathbf{R}_{C_j}^W. \quad (21)$$

Note that  $[\mathbf{a}_{ij} \times]^4 = \mathbf{I} - \mathbf{a}_{ij} \mathbf{a}_{ij}^T$ , so we rewrite Eq. (14) as

$$\begin{aligned} & \left( \sum_{j \in \mathcal{A}_i} \mathbf{R}_W^{C_j} (\mathbf{I} - \mathbf{a}_{ij} \mathbf{a}_{ij}^T) \mathbf{R}_{C_j}^W \right) \mathbf{X}_i \\ &= \sum_{j \in \mathcal{A}_i} \mathbf{R}_W^{C_j} (\mathbf{I} - \mathbf{a}_{ij} \mathbf{a}_{ij}^T) \mathbf{R}_{C_j}^W \mathbf{c}_j \end{aligned} \quad (22)$$

which is precisely the formulation for the midpoint triangulation in  $n$ -view [56]. The proof for the resection case is analogous. We still note that LOSTU is a more general framework that can treat camera position uncertainties of different amplitudes alongside angular noise. Thereafter, midpoint refers to the algorithm solving Eq. (22).

### 3. Triangulation in SfM framework

Structure from Motion (SfM) is the process of reconstructing a 3D scene from 2D images. This process is also commonly used for Simultaneous Localization and Mapping (SLAM) although SLAM is a more general concept that can work with other types of measurements and also

emphasizes the position of the observer [5, 29]. Today's SfM pipelines have matured considerably since early work [39, 54], and are now routinely used to reconstruct large urban scenes [1, 50–52], terrain [60], and celestial bodies [15, 47]. This section is aimed at pointing out the particular aspects to consider when triangulating in SfM.

There are many different approaches when it comes to SfM, but all have in common that features need to be extracted from—and matched between—images. This process can be done by well-known handcrafted algorithms [2, 40, 41, 49] or learning algorithms [13, 43, 48]. In some cases the 2D uncertainty that comes with those features can be rigorously estimated, though it is also common to simply assume a fixed value (*e.g.*, 1 pixel). From here, we often categorize distinct approaches.

**Sequential SfM** The extracted features are used to estimate an initial relative pose between at least two starting views. This seeding process is preferably done in a dense central place [20]. This process can be done with the five point algorithm [46] for calibrated cameras or the eight point algorithm [21] for uncalibrated cameras, which are often coupled with an outlier detection scheme like RANSAC [17]. The 3D points commonly seen by the cameras can be triangulated. Then, an initial bundle adjustment (BA) allows one to obtain the initial covariance of the poses and structure [23, 57].

Views are then added sequentially. Several options exist when it comes to selecting the next best view. It can involve propagating the covariance and selecting the best camera, but this is slow in practice since it requires many unnecessary view estimations. Instead, simple rules like choosing the camera that sees the most points work well in practice [20]. The estimation of a view pose using 3D points is referred to as the *Perspective- $n$ -Point* (PnP). The PnP problem can be solved using from 3 [14, 18, 19] to  $n$  [23, 32, 37, 63] measurements, and the reprojection error is often the quantity minimized, but these break the pattern of maximum-likelihood since not all uncertainties are taken into account. Other works propose to leverage uncertainties from the 3D reconstructed points directly in the PnP *e.g.* [16, 28, 58, 59]. The view pose uncertainties arising from a process like the one in Ref. [59] can be obtained because they use a subsequent iterative refinement with Levenberg-Marquardt (LM) or Gauss-Newton (GN).

Once a camera is added, all points seen by two views or more are triangulated. The choice of the best triangulation method depends on the magnitude of the pose noise and availability/accuracy of the pose covariance, and the triangulation covariance expressions [26] can help in the analysis.

Depending on the parameters, either a BA step is performed, or the next view is estimated. Careful implemen-



tations can greatly reduce the computational load of BA [50, 61]. There are often additional triangulation steps before and after bundle adjustment [50]. Depending on the reconstruction, obtaining the covariance of the poses after BA may be practically difficult. If the covariance are not obtainable, BA still reduces the errors of the poses and thus may render  $L_2$  triangulation more profitable.

**Global SfM** Sequential SfM, although very accurate, can be slow. Popular and faster alternatives are global SfM [7, 44, 55] that estimate all poses first, triangulate, and then perform bundle adjustment only once. After estimating relative poses with aforementioned tools, the *averaging* process refines them into a coherent set [6, 7, 11, 24]. Ref. [62] propagates uncertainties into weights for estimated rotations. This may be particularly interesting to use in conjunction with LOSTU.

**Hybrid SfM** A proposed middle-ground to sequential or global SfM is *hybrid* SfM [9, 12], where all camera rotations are first estimated, and the sequential part only focuses on camera center and structure reconstruction. In this case, the problem reduces to a sequence of triangulation problems. The LOST framework allows to seamlessly obtain the optimal camera center using the 3D structure as in Sec. 2.1, and 3D structure using camera centers as in Sec. 2.2.

## 4. Triangulation experiments

### 4.1. Two-view triangulation

Many applications in 3D vision and navigation use a limited number of cameras. The case of solving 2-view triangulation has been widely discussed in the literature [25, 31, 38]. In this section, we compare the performance of LOST against the 6th order polynomial of Hartley and Sturm (HS [25]), the fast optimal solution developed by Lindstrom (niter2 [38]), DLT, midpoint, and LOSTU (the only solution here that takes into account camera pose uncertainties). The purpose of this experiment is double. First, it shows that directly solving the simple LOST linear system gives essentially the same result as the more complicated (and slower) Hartley and Sturm polynomial. Second, it aims to address the findings in [35, 45] that tested optimal triangulation in geometries where optimal triangulation simply has no advantage.

Suppose a 3D object is placed at the origin and observed by two cameras that are placed in  $c_1 = [0, y_1, z_1]^T$  and  $c_2 = [0, -2, -2]^T$ . In the nominal case, camera one is placed such that  $y_1 = -2$ ,  $z_1 = -6$ . The camera has an effective focal length of 400. We assume a 2D noise of  $\sigma_{px} = 1$  pixel, a camera rotation noise of  $\sigma_\phi = 0.5$  deg, and a camera center noise of  $\sigma_c = 0.03$ . The cameras are rotated such that they point towards the 3D point (orbital configuration).

Independently, we vary  $\sigma_x$ , the camera pose,  $y_1$ , and  $z_1$ . To make the results more graphically meaningful, we show the results in Fig. 2 in percentage of position RMSE compared to the HS polynomial solution:

$$\text{Error} = 100 \times (\text{RMSE}_\tau - \text{RMSE}_{\text{HS}}) / \text{RMSE}_{\text{HS}}, \quad (23)$$

where  $\tau$  is the tested triangulation method. Fig. 2a highlights the gap in performance between the optimal solutions and midpoint or DLT.

The fact that a performance gap persists when there is no pixel noise is due to the remaining uncertainty in the camera pose. In Fig. 2b, we observe that the non-optimal algorithms get better relative to the polynomial solution of Hartley and Sturm as the camera pose uncertainties increase. We also observe that LOST behaves comparatively better in that case, and LOSTU always has the lowest error. When there are no camera pose uncertainties, all optimal methods have the same RMSE. Fig. 2c confirms the analysis of Eq. (15) in that the sub-optimal methods behave similarly to the optimal methods at  $z_1 = -2$ , when the geometry is symmetric and the ranges are all the same. As the depth decreases, the relative importance of the camera center noise increases and midpoint performs well. Finally, Fig. 2d shows what happens when the angle between the two observations progressively decrease. In this case we observe that the classical two view optimal solutions, HS and niter2, start to comparatively lose in quality. This trend is less pronounced if no camera noise is added. LOST and LOSTU exhibit better behavior in low parallax.

This prompts us to investigate the low parallax behavior of LOST compared to standard methods like HS. This experiment is done without camera pose noise. Set  $c_1 = [1, 0, -6]$  and  $c_2 = [1, 0, -5]$ , such that the inter line-of-sight angle is less than 2 degree. As pixel noise increases, both HS and niter2 become unstable, whereas LOST stays on par with the DLT and the midpoint methods. The results for this experiment and a standard deviation of 1 pixel is available in Tab. 1. Other two-view triangulation techniques can be considered when low parallax is the main focus [35].

The runtimes of the tested algorithms are presented in Tab. 2. The experiment has been performed with MATLAB and a 2.3 GHz Intel Core i9. Our MATLAB implementation of the niter2 by Lindstrom [38] remains the fastest method to triangulate optimally in two view. LOST is still twice as fast as solving the HS and comes with additional robustness and scalability benefits.

This experiment shows that optimal triangulation can still lead to improvements over non-optimal schemes, even when substantial camera pose uncertainties exist. It does show operational regions where standard optimal triangulation algorithms become less stable. The LOST algorithm gives a similar solution to standard  $L_2$  triangulation in nom-

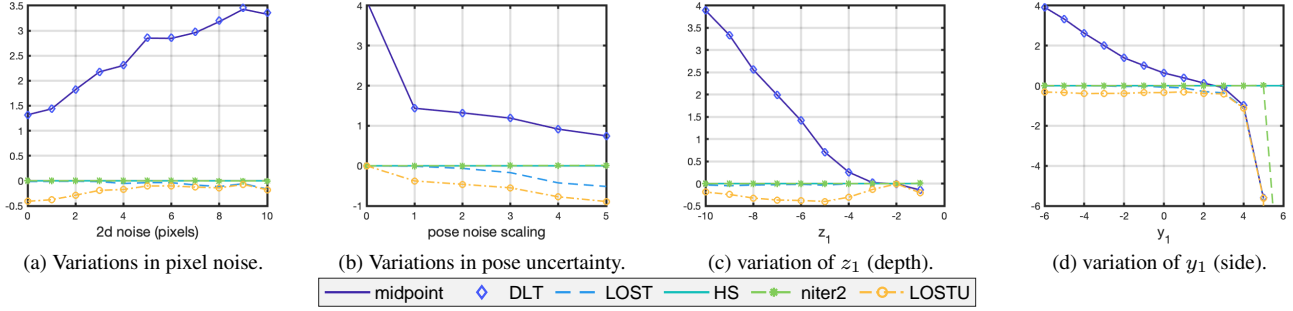


Figure 2. Percentage of RMSE deterioration with respect to HS for two view triangulation. The curves for DLT and midpoint are on top of each other. We distinguish a clear demarcation between optimal and suboptimal methods.

inal cases, while also responding better to camera noise and low parallax.

midpoint	DLT	LOST	HS	niter2
0.6280	0.6280	0.6280	0.6470	0.6470

Table 1. RMSE two-view triangulation methods at low parallax.

midpoint	DLT	LOST	HS	niter2	LOSTU
12.8	19.9	23.5	52.4	12.9	43.7

Table 2. Mean runtimes of different triangulation methods, in  $\mu$ s.

## 4.2. N-view triangulation

This experiment aims to compare multiple triangulation solutions in a typical SfM geometry. The algorithms selected are midpoint, DLT, LOST as the  $L_2$  optimal triangulation, and LOSTU as the triangulation accounting for all uncertainties. The DLT method is also implemented with a refinement using factor graphs and LM [10] to minimize either the reprojection error with DLT+LM (reproj), or the Mahalanobis distance DLT+LM (Mahalanobis). For comparison, a DLT solution that is refined by LOSTU is also added, DLT+LOSTU.

A single point placed at  $X = [2, 1, 0]$  is triangulated by  $m = 50$  cameras randomly spawned in a domain  $\mathcal{D}_{\text{cam}} = \{[x_{\min}, x_{\max}] = [-10, 10], [y_{\min}, y_{\max}] = [-10, 10], [z_{\min}, z_{\max}] = [-50, -10]\}$ . Each camera is oriented to look in the  $+z$  direction with a random deviation of 2deg. The effective focal length of the camera is 800 and an isotropic 2D noise of 1 pixel is added to the measurements. Furthermore, a camera rotation noise of  $\sigma_\phi = 0.05\text{deg}$  and translation of  $\sigma_c = 0.02$  is added for every camera. These pose uncertainties are randomly scaled by a factor from 1/2 to 2 for each camera, so that all cameras do not have the same uncertainties.

Each of the parameters will be varied independently to study their effects on classical triangulation solutions. For each set of parameters, we perform triangulation 5000 times, where camera poses and measurements are regenerated at each iteration. The position RMSE are recorded in Fig. 3 while the mean runtimes are displayed in Fig. 4.

One can observe that midpoint is the fastest method but it provides a suboptimal solution, except when the position uncertainty of the cameras dominate, which confirms the results in Sec. 2.3. The midpoint will not coincide with the optimal solution for high camera center noise because cameras have different pose noise. The DLT is slower, but still time-efficient, and it is consistently better than the midpoint in this experiment. Minimizing the reprojection error is still a strategy that yields significant improvements over DLT and midpoint, depending on multiple factors. First, the geometries favouring greater variations in distance between the views give an edge to  $L_2$  triangulation. Second, noise in the position of the camera centers reduce the relative performance of  $L_2$  triangulation. Third, the number of views may change the relative performance between methods. In our findings, a moderate number of views tend to favor minimizing the reprojection error, and then the relative performance may go in either direction depending on the 2D noise to pose noise ratio. LOST performs statistically identically to the LM refinement at a fraction of the computational cost. This behavior slightly deviates for a high number of views when the angular noise becomes significant, probably due to the fact that the weighting is done by estimating the range using noisy measurements.

All the methods above do not require any knowledge of the covariance matrices. When these are available, the methods that properly account for them are always statistically better, sometimes substantially so. LOSTU again performs equivalently to the LM refinement, and can be slightly more robust if used in a refinement way. As a final implementation tip, LOSTU can be made as fast as LOST if the residual covariance matrix in Eq. (8) is approximated by a diagonal matrix to speed-up the computation of the

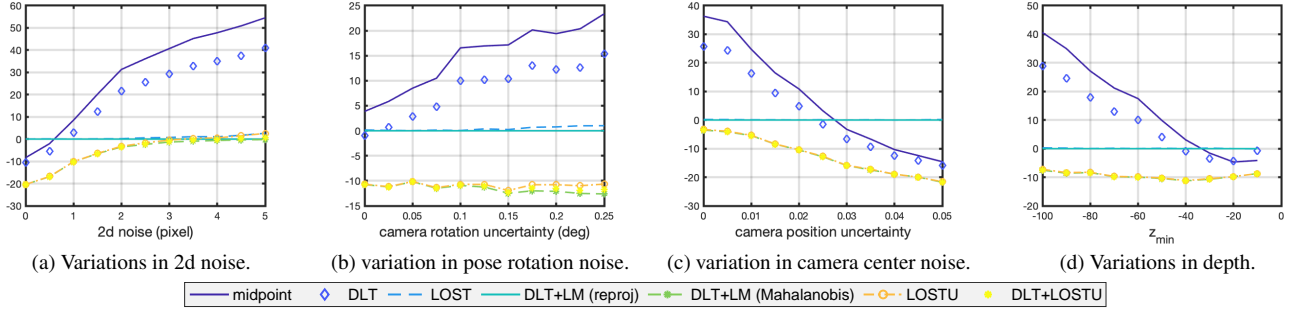


Figure 3. Percentage of RMSE deterioration with respect to DLT+LM (reproj) for 50-view triangulation.

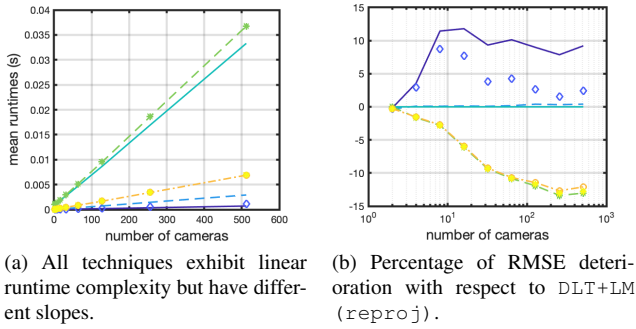


Figure 4. Evolution of triangulation as the number of views increases. Legends can be found in Fig. 3

pseudo-inverse. In that case the results were found to still be close to the standard LOSTU.

## 5. Sequential reconstruction example

Reference [20] proposed a reconstruction pipeline where cameras and points are sequentially added and covariance propagated throughout. In their approach, cameras are iteratively refined to the maximum likelihood estimate when they are estimated for the first time. Cameras are not accepted if their reprojection error is too large. Points seen by at least two views are triangulated and iteratively refined to a maximum likelihood estimate. Similarly, points are not accepted if their reprojection error and covariance are too large. While bundle adjustment often remains necessary for the most accurate reconstructions, this way of reconstructing has been shown to yield decent sequential reconstructions without it. We choose to follow a similar setup to build a reconstruction problem where the camera poses have an estimated covariance. This allows us to then compare the performance of different triangulation solutions.

For camera pose estimation, we distinguish cases where the reprojection error is minimized with EPnP [37] (and the covariance does *not* correctly account for all terms) vs. the case where 3D point uncertainties are also taken into

account in EPnP [59] (the covariance is correctly propagated). We test the following configurations: 1) EPnP+DLT (standard practice), 2) EPnP+LOST (minimized reprojection error), 3) EPnP+DLT (correct covariance propagation), and 4) EPnP+LOSTU (correct covariance propagation and maximum likelihood solution). Two datasets are used. First, Notre Dame (ND) whose surface is planar, but a lot of views have different ranges to the 3D points. Second, the RC3b segment around the Vesta asteroid, where views are in an orbital configuration and cannot see the other side of the structure.

### 5.1. Notre Dame

The West facade of Notre-Dame de Paris (ND) is a very common dataset for triangulation [51]. Starting from two views with 700 SIFT keypoints in common, we estimate their relative pose along with a RANSAC scheme to find inliers. Inliers are then triangulated and the initial pose uncertainty is estimated with BA. The next best view is chosen as the camera that observes the most estimated points. If the reconstructed camera has a mean reprojection error higher than 5 pixels, then it is not considered until 3D points are better refined, and another camera is estimated instead. Points are re-triangulated as more views are added. 3D points whose reprojection error is higher than 5 pixels, or standard deviation  $\sigma_X = \sqrt{\text{trace}(\Sigma_X)}$  exceeds about 3 m (scale assumed known) are not accepted. An initial 2D standard deviation of 1 pixel is assumed to compute the initial covariances—this value is only a guess of the true value. While the reprojection error is not the metric to minimize for maximum likelihood, it is still a convenient representation of the global condition of the reconstruction that does not require covariance to be computed.

As results in Tab. 3 suggest, we observe that the solutions that do not properly propagate the covariance exhibit worse reconstruction metrics. Since no BA is performed in this experiment, camera pose noise remains high and minimizing the reprojection error in the triangulation step does not coincide with a maximum likelihood estimate anymore. LOST still performed marginally better than DLT when looking at

Simulation	estimated points	estimated cameras	time (s)	reprojection error (pixels)	3D reconstruction errors		
					$\mu_E$	$\sigma_E$	RMSE
ND Dataset	127431	715	-	0.514	-	-	-
EPnP+DLT	116,665	612	683	0.745	0.0246	0.0361	0.0436
EPnP+LOST	125,909	655	637	0.749	0.0238	0.0208	0.0316
EPnPU+DLT	111,570	632	511	0.603	0.0211	0.0108	<b>0.0237</b>
EPnPU+LOSTU	117,129	686	613	0.602	0.0212	0.0106	<b>0.0237</b>
Vesta (ground truth+LOST)	37,205	65	-	0.768	-	-	-
EPnPU+DLT	10,396	24	22	1.104	2.0715	4.5874	5.0332
EPnPU+LOSTU	28,865	58	49	0.929	1.0988	0.9748	<b>1.4688</b>

Table 3. Reconstruction metrics for ND and Vesta. The mean reprojection error is represented. The 3D errors are only for the points commonly estimated by all methods, with respect to the Dataset for ND and ground truth+LOST for Vesta.

the reconstruction errors and estimated cameras. When covariance propagation is properly taken into account, LOSTU resulted in the triangulation of 5,000 more points and 50 more cameras than the DLT, while simultaneously producing a lower 3D error. Fig. 6 shows the initial evolution of the reprojection error as more cameras are added. We observe that LOST does indeed give the lowest reprojection error in short term propagation from the initial bundle adjustment. However, using maximum likelihood techniques exhibit better behavior in the long term, as uncertainties tend to grow without regular BA.

Overall, this experiment shows that correct estimation and propagation of the covariance in triangulation can lead to results that are closer the reconstructed dataset. Depending on the required fidelity of the reconstruction, this can lead to a simple SfM pipeline with reduced need for BA. These conclusions are similar to those found in Ref. [20].

## 5.2. Vesta reconstruction

The Astrovision dataset [15] offers the possibility to reconstruct several asteroids. We choose the ASLFeat features [43] trained on Astrovision data, *ASLFeat-CVGBEDTRPJM*, since these were shown to extract a large number of features with good precision on asteroid images. After matching and outlier rejection, we perform the sequential SfM to 3D reconstruct Vesta. The maximum reprojection error to accept a camera or a point is set to 5 pixels. The maximum covariance to accept a 3D point is set to a value such that the reconstructed surface looks arbitrarily smooth. Results for EPnPU+DLT versus EPnPU+LOSTU are found in Tab. 3, and the visual in Fig. 1, in which we observe that LOSTU estimated more than double the number of cameras and points compared to DLT. The mean reprojection and reconstruction errors are lower in the case of LOSTU.

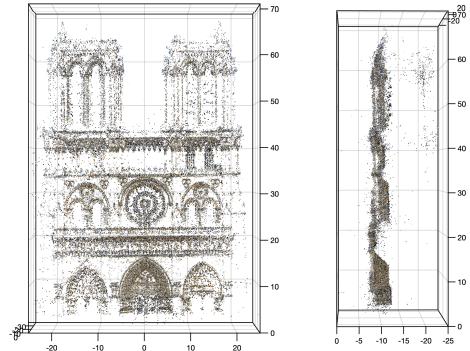


Figure 5. Reconstructed solution for ND using EPnPU+LOSTU.

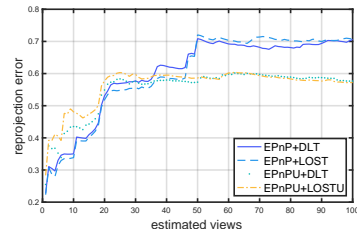


Figure 6. Evolution of the reprojection errors for ND without bundle adjustment.

## 6. Conclusion

This work developed optimal and scalable triangulation methods for 3D reconstruction. Geometry, the number of views, and the relative weight of camera parameters to 2D noise all play a crucial role when choosing the right triangulation method. When information on the uncertainties is available, LOSTU can lead to substantial improvements. However, finding accurate pose covariances from images can be challenging, and there remains room for improvement in how easily these could be obtained.



**Acknowledgements** We thank Travis Driver for his help in the asteroid reconstruction example and valuable feedback on this manuscript. We also thank Michael Krause and Priyal Soni for their thoughtful comments.

## References

- [1] Sameer Agarwal, Yasutaka Furukawa, Noah Snavely, Ian Simon, Brian Curless, Steven M. Seitz, and Richard Szeliski. Building rome in a day. *Commun. ACM*, 54(10):105–112, 2011. 4
- [2] Herbert Bay, Andreas Ess, Tinne Tuytelaars, and Luc Van Gool. Speeded-up robust features (surf). *Computer Vision and Image Understanding*, 110(3):346–359, 2008. Similarity Matching in Computer Vision and Multimedia. 4
- [3] A.S. Bedekar and R.M. Haralick. A bayesian method for triangulation and its application to finding corresponding points. In *Proceedings., International Conference on Image Processing*, pages 362–365 vol.2, 1995. 2
- [4] Martin Byröd, Klas Josephson, and Kalle Åström. Fast optimal three view triangulation. In *Computer Vision – ACCV 2007*, pages 549–559, Berlin, Heidelberg, 2007. Springer Berlin Heidelberg. 1
- [5] Carlos Campos, Richard Elvira, Juan J. Gómez Rodríguez, José M. M. Montiel, and Juan D. Tardós. Orb-slam3: An accurate open-source library for visual, visual–inertial, and multimap slam. *IEEE Transactions on Robotics*, 37(6):1874–1890, 2021. 4
- [6] Avishek Chatterjee and Venu Madhav Govindu. Efficient and robust large-scale rotation averaging. In *2013 IEEE International Conference on Computer Vision*, pages 521–528, 2013. 5
- [7] Yu Chen, Ji Zhao, and Laurent Kneip. Hybrid rotation averaging: A fast and robust rotation averaging approach. In *2021 IEEE/CVF Conference on Computer Vision and Pattern Recognition (CVPR)*, pages 10353–10362, 2021. 5
- [8] John A. Christian. A tutorial on horizon-based optical navigation and attitude determination with space imaging systems. *IEEE Access*, 9:19819–19853, 2021. 3
- [9] Hainan Cui, Xiang Gao, Shuhan Shen, and Zhanyi Hu. Hsfm: Hybrid structure-from-motion. In *2017 IEEE Conference on Computer Vision and Pattern Recognition (CVPR)*, pages 2393–2402, 2017. 5
- [10] Frank Dellaert. Factor graphs and gtsam: A hands-on introduction. 2012. 6
- [11] Frank Dellaert, David M. Rosen, Jing Wu, Robert Mahony, and Luca Carlone. Shonan rotation averaging: Global optimality by surfing  $SO(p)^n$ . In *Computer Vision – ECCV 2020*, pages 292–308, Cham, 2020. Springer International Publishing. 5
- [12] Kaitlin Dennison and Simone D’Amico. Leveraging camera attitude priors for structure from motion of small, noncooperative targets. In *2023 AAS/AIAA Astrodynamics Specialist Conference*, 2023. 5
- [13] Daniel DeTone, Tomasz Malisiewicz, and Andrew Rabinovich. Superpoint: Self-supervised interest point detection and description. In *2018 IEEE/CVF Conference on Computer Vision and Pattern Recognition Workshops (CVPRW)*, pages 337–33712, 2018. 4
- [14] M. Dhome, M. Richetin, J.-T. Lapreste, and G. Rives. Determination of the attitude of 3d objects from a single perspective view. *IEEE Transactions on Pattern Analysis and Machine Intelligence*, 11(12):1265–1278, 1989. 4
- [15] Travis Driver, Katherine A. Skinner, Mehregan Dor, and Panagiotis Tsiotras. Astrovision: Towards autonomous feature detection and description for missions to small bodies using deep learning. *Acta Astronautica*, 210:393–410, 2023. 1, 4, 8
- [16] Luis Ferraz Colomina, Xavier Binefa, and Francesc Moreno-Noguer. Leveraging feature uncertainty in the pnp problem. In *Proceedings of the BMVC 2014 British Machine Vision Conference*, pages 1–13, 2014. 4
- [17] Martin A. Fischler and Robert C. Bolles. Random sample consensus: A paradigm for model fitting with applications to image analysis and automated cartography. *Commun. ACM*, 24(6):381–395, 1981. 4
- [18] Xiao-Shan Gao, Xiao-Rong Hou, Jianliang Tang, and Hang-Fei Cheng. Complete solution classification for the perspective-three-point problem. *IEEE Transactions on Pattern Analysis and Machine Intelligence*, 25(8):930–943, 2003. 4
- [19] J. A. Grunert. Das Pothenot’sche Problem in erweiterter Gestalt; nebst Bemerkungen über seine Anwendungen in der Geodisie. *Archiv der Mathematik und Physik*, 1:238–248, 1841. 4
- [20] Sebastian Haner and Anders Heyden. Covariance propagation and next best view planning for 3d reconstruction. In *Computer Vision – ECCV 2012*, pages 545–556, Berlin, Heidelberg, 2012. Springer Berlin Heidelberg. 2, 4, 7, 8
- [21] R.I. Hartley. In defense of the eight-point algorithm. *IEEE Transactions on Pattern Analysis and Machine Intelligence*, 19(6):580–593, 1997. 4
- [22] R. Hartley and F. Schaffalitzky.  $L_{\text{sub}/\text{spl}}/\infty$  minimization in geometric reconstruction problems. In *Proceedings of the 2004 IEEE Computer Society Conference on Computer Vision and Pattern Recognition, 2004. CVPR 2004.*, pages I–I, 2004. 1
- [23] Richard Hartley and Andrew Zisserman. *Multiple View Geometry in Computer Vision*. Cambridge University Press, 2 edition, 2004. 1, 4
- [24] Richard Hartley, Jochen Trumpf, Yuchao Dai, and et al. Rotation averaging. *International Journal of Computer Vision*, 103:267–305, 2013. 5
- [25] R. I. Hartley and P. Sturm. Triangulation. *Computer Vision and Image Understanding*, 68(2):146–157, 1997. 1, 2, 5
- [26] Sébastien Henry and John A. Christian. Absolute triangulation algorithms for space exploration. *Journal of Guidance, Control, and Dynamics*, 46(1):21–46, 2023. 1, 2, 3, 4
- [27] Sébastien Henry and John A. Christian. Analytical methods in triangulation-based celestial localization. *Journal of Astronautical Sciences*, 70(37), 2023. 2
- [28] Saeed Jahani, Mahsa Shoaran, and Golnoosh Karimian Khosroshahi. AQPnP: an accurate and quaternion-based

- solution for the perspective-n-point problem. *The Visual Computer*, 2023. 4
- [29] Michael Kaess, Ananth Ranganathan, and Frank Dellaert. isam: Incremental smoothing and mapping. *IEEE Transactions on Robotics*, 24(6):1365–1378, 2008. 4
- [30] Fredrik Kahl and Richard Hartley. Multiple-view geometry under the  $L_\infty$ -norm. *IEEE Transactions on Pattern Analysis and Machine Intelligence*, 30(9):1603–1617, 2008. 1
- [31] K. Kanatani, Y. Sugaya, and H. Niitsuma. Triangulation from two views revisited: Hartley-sturm vs. optimal correction. In *Proceedings of the British Machine Vision Conference*, pages 18.1–18.10. BMVA Press, 2008. 1, 5
- [32] Laurent Kneip, Hongdong Li, and Yoon Seo. Upnp: An optimal  $O(n)$  solution to the absolute pose problem with universal applicability. In *Computer Vision – ECCV 2014*. Springer, Cham, 2014. 4
- [33] Akshay Krishnan, Sebastien Henry, Frank Delbart, and John Christian. Lost in triangulation. <https://gtsam.org/2023/02/04/lost-triangulation.html>, 2023. 2
- [34] Zuzana Kukelova, Tomas Pajdla, and Martin Bujnak. Fast and stable algebraic solution to 12 three-view triangulation. In *2013 International Conference on 3D Vision - 3DV 2013*, pages 326–333, 2013. 1
- [35] Seong Hun Lee and Javier Civera. Triangulation: Why optimize?, 2019. 2, 5
- [36] Seong Hun Lee and Javier Civera. Robust uncertainty-aware multiview triangulation. *arXiv preprint arXiv:2008.01258*, 2020. 2
- [37] Vincent Lepetit, Francesc Moreno-Noguer, and Pascal Fua. Epnp: An accurate  $O(n)$  solution to the pnp problem. *International Journal of Computer Vision*, 81(2):155–166, 2009. 4, 7
- [38] Peter Lindstrom. Triangulation made easy. In *2010 IEEE Computer Society Conference on Computer Vision and Pattern Recognition*, pages 1554–1561, 2010. 1, 5
- [39] H.C. Longuet-Higgins. A computer algorithm for reconstructing a scene from two projections. *Nature*, 293:133–135, 1981. 4
- [40] D.G. Lowe. Object recognition from local scale-invariant features. In *Proceedings of the Seventh IEEE International Conference on Computer Vision*, pages 1150–1157 vol.2, 1999. 4
- [41] David G. Lowe. Distinctive image features from scale-invariant keypoints. *International Journal of Computer Vision*, 60:91–110, 2004. 4
- [42] Fangfang Lu and Richard Hartley. A fast optimal algorithm for 12 triangulation. In *Computer Vision – ACCV 2007*, pages 279–288, Berlin, Heidelberg, 2007. Springer Berlin Heidelberg. 2
- [43] Zixin Luo, Lei Zhou, Xuyang Bai, Hongkai Chen, Jiahui Zhang, Yao Yao, Shiwei Li, Tian Fang, and Long Quan. Aslfeat: Learning local features of accurate shape and localization. In *2020 IEEE/CVF Conference on Computer Vision and Pattern Recognition (CVPR)*, pages 6588–6597, 2020. 4, 8
- [44] Pierre Moulon, Pascal Monasse, and Renaud Marlet. Global fusion of relative motions for robust, accurate and scalable structure from motion. In *2013 IEEE International Conference on Computer Vision*, pages 3248–3255, 2013. 5
- [45] Seyed-Mahdi Nasiri, Reshad Hosseini, and Hadi Moradi. The optimal triangulation method is not really optimal. *IET Image Processing*, 17(10):2855–2865, 2023. 2, 4, 5
- [46] D. Nister. An efficient solution to the five-point relative pose problem. *IEEE Transactions on Pattern Analysis and Machine Intelligence*, 26(6):756–770, 2004. 4
- [47] Eric E. Palmer, Robert Gaskell, Michael G. Daly, Olivier S. Barnouin, Coralie D. Adam, and Dante S. Lauretta. Practical stereophotoclinometry for modeling shape and topography on planetary missions. *The Planetary Science Journal*, 3(5): 102, 2022. 4
- [48] Jerome Revaud, Cesar De Souza, Martin Humenberger, and Philippe Weinzaepfel. R2d2: Reliable and repeatable detector and descriptor. In *Advances in Neural Information Processing Systems*. Curran Associates, Inc., 2019. 4
- [49] Ethan Rublee, Vincent Rabaud, Kurt Konolige, and Gary Bradski. Orb: An efficient alternative to sift or surf. In *2011 International Conference on Computer Vision*, pages 2564–2571, 2011. 4
- [50] Johannes L. Schönberger and Jan-Michael Frahm. Structure-from-motion revisited. In *2016 IEEE Conference on Computer Vision and Pattern Recognition (CVPR)*, pages 4104–4113, 2016. 4, 5
- [51] Noah Snavely, Steven M. Seitz, and Richard Szeliski. Photo tourism: Exploring photo collections in 3d. *ACM Trans. Graph.*, 25(3):835–846, 2006. 7
- [52] Noah Snavely, Steven M. Seitz, and Richard Szeliski. Modeling the world from internet photo collections. *International Journal of Computer Vision*, 80:189–210, 2008. 4
- [53] H. Stewenius, F. Schaffalitzky, and D. Nister. How hard is 3-view triangulation really? In *Tenth IEEE International Conference on Computer Vision (ICCV’05) Volume 1*, pages 686–693 Vol. 1, 2005. 1
- [54] I.E. Sutherland. Three-dimensional data input by tablet. *Proceedings of the IEEE*, 62(4):453–461, 1974. 4
- [55] Christopher Sweeney, Tobias Hollerer, and Matthew Turk. Theia: A fast and scalable structure-from-motion library. In *Proceedings of the 23rd ACM International Conference on Multimedia*, page 693–696, New York, NY, USA, 2015. Association for Computing Machinery. 5
- [56] Richard Szeliski. *Computer vision: algorithms and applications*. Springer Cham, 2022. 4
- [57] Bill Triggs, Philip F. McLauchlan, Richard I. Hartley, and Andrew W. Fitzgibbon. Bundle adjustment — a modern synthesis. In *Vision Algorithms: Theory and Practice*, pages 298–372, Berlin, Heidelberg, 2000. Springer Berlin Heidelberg. 4
- [58] S. Urban, J. Leitloff, and S. Hinz. Mlpnp - a real-time maximum likelihood solution to the perspective-n-point problem. *ISPRS Annals of the Photogrammetry, Remote Sensing and Spatial Information Sciences*, III-3:131–138, 2016. 4
- [59] Alexander Vakhitov, Luis Ferraz Colomina, Antonio Agudo, and Francesc Moreno-Noguer. Uncertainty-aware camera

- pose estimation from points and lines. In *2021 IEEE/CVF Conference on Computer Vision and Pattern Recognition (CVPR)*, pages 4657–4666, 2021. 4, 7
- [60] M.J. Westoby, J. Brasington, N.F. Glasser, M.J. Hambrey, and J.M. Reynolds. ‘structure-from-motion’ photogrammetry: A low-cost, effective tool for geoscience applications. *Geomorphology*, 179:300–314, 2012. 4
- [61] Changchang Wu. Towards linear-time incremental structure from motion. In *2013 International Conference on 3D Vision - 3DV 2013*, pages 127–134, 2013. 5
- [62] Ganlin Zhang, Viktor Larsson, and Daniel Barath. Revisiting rotation averaging: Uncertainties and robust losses. In *2023 IEEE/CVF Conference on Computer Vision and Pattern Recognition (CVPR)*, pages 17215–17224, 2023. 5
- [63] Yinqiang Zheng, Yubin Kuang, Shigeki Sugimoto, Kalle Åström, and Masatoshi Okutomi. Revisiting the pnp problem: A fast, general and optimal solution. In *2013 IEEE International Conference on Computer Vision*, pages 2344–2351, 2013. 4